Submicroscopic Deletions at 13q32.1 Cause Congenital Microcoria.

Lucas Fares-Taie, Sylvie Gerber, Akihiko Tawara, Arturo Ramirez-Miranda, Jean-Yves Douet, Hannah Verdin, Antoine Guilloux, Juan C Zenteno, Hiroyuki Kondo, Hugo Moisset, et al.

Report

Submicroscopic deletions at 13q32.1 cause congenital microcoria

Lucas Fares-Taie[1], Sylvie Gerber[1], Akihiko Tawara[2†], Arturo Ramirez-Miranda[3†], Jean-Yves Douet[4†], Hannah Verdin[5], Antoine Guilloux[1], Juan C. Zenteno[6], Hiroyuki Kondo[2], Hugo Moisset[1], Bruno Passet[7], Ken Yamamoto[8], Masaru Iwai[9,10], Toshihiro Tanaka[11,12,13], Yusuke Nakamura[14], Wataru Kimura[15], Christine Bole-Feysot[16], Marthe Vilotte[7], Sylvie Odent[17], Jean-Luc Vilotte[7], Arnold Munnich[1], Alain Regnier[4], Nicolas Chassaing[18], Elfride De Baere[5], Isabelle Raymond-Letron[4], Josseline Kaplan[1], Patrick Calvas[18], Olivier Roche[19]*, Jean-Michel Rozet[1]*

[1]Laboratory of Genetics in Ophthalmology (LGO). INSERM UMR1163. *Imagine* – Institute of Genetic Diseases, Paris Descartes University, 75015 Paris, France

[2]Department of Ophthalmology, University of Occupational & Environmental Health, Kitakyushu 807-8555, Japan

[3]Department of Cornea And Refractive Surgery, Instituto de Oftalmologia “Conde de Valenciana”. UNAM, Mexico City, DF 06800, Mexico

[4]Veterinary School of Toulouse, University of Toulouse, 31300 Toulouse, France

[5]Center for Medical Genetics, Ghent University, 9000 Ghent, Belgium

[6]Department of Genetics-Research Unit, Instituto de Oftalmologia “Conde de Valenciana” And Department of Biochemistry, Faculty of Medicine, UNAM, Mexico City, DF 06800, Mexico

[7]UMR1313 Génétique Animale et Biologie Intégrative, Institut Nationale de la Recherche Agronomique, 78352 Jouy-en-Josas, France

[8]Division of Genome Analysis, Institute of Bioregulation, Kyushu University, Fukuoka 812-8582 Japan

[9]Department of Molecular Cardiovascular Biology and Pharmacology. Ehime University Graduate School of Medicine, Ehime 791-0295, Japan

[10]National Hospital Organization, Ehime Medical Center, Tohon, Ehime 791-0281, Japan

[11]Department of Human Genetics and Disease Diversity, Graduate School of Medical and Dental Sciences, Tokyo Medical and Dental University, 113-0034 Tokyo, Japan

[12]Division of Disease Diversity, Bioresource Research Center, Tokyo Medical and Dental University, 113-0034 Tokyo, Japan

[13]Laboratory for Cardiovascular Diseases, RIKEN Center for Integrative Medical Sciences, Yokohama, Kanagawa 230-0045, Japan

[14]Department of Medicine and Surgery, The University of Chicago, 5801 South Ellis Avenue, Chicago, Illinois 60637, USA

[15]Kimura Eye Clinic, Kure 737-0046 Japan

[16]Genomics Plateform, IMAGINE Foundation and Paris Descartes University, 75015 Paris, France

[17]Service de Génétique Clinique, CHU Hôpital Sud, 35203 Rennes, France

[18]Service de Génétique Clinique, Hôpital Purpan, 31300 Toulouse, France

[19]Department of Ophthalmology, IHU Necker-Enfants Malades, University Paris-Descartes, 75015 Paris, France

†AT, ARM and JYD contributed equally to this work

*OR and JMR contributed equally to this work

Correspondence to oph.roche@free.fr or jean-michel.rozet@inserm.fr

Abstract

Congenital microcoria (MCOR) is a rare autosomal dominant disorder characterized by inability of the iris to dilate owing to absence of dilator pupillae muscle. So far, a dozen MCOR families are reported worldwide. By using whole-genome oligonucleotide array CGH, we have identified deletions at 13q32.1 segregating with MCOR in six families originating from France, Japan and Mexico. Breakpoint sequence analyses showed nonrecurrent deletions in 5/6 families. The deletions varied from 35 Kbp to 80 Kbp in size, but invariably encompassed or interrupted only two genes: *TGDS* encoding the TDP-glucose 4,6-dehydratase and *GPR180* encoding the G protein-coupled receptor 180, also known as intimal thickness-related receptor (ITR). Unlike TGDS which has no known function in muscle cells, GPR180 is involved in the regulation of smooth muscle cell growth. The identification of a null *GPR180* mutation segregating over two generations with iridocorneal angle dysgenesis which can be regarded as a MCOR endophenotype is consistent with the view that deletions of this gene, with or without the loss of elements regulating the expression of neighboring genes, are the cause of MCOR.

Main text

Inherited congenital microcoria (MCOR) [MIM156600], also referred to as congenital miosis, is a rare inborn error of iris development. It is characterized by a small pupil (diameter < 2 mm) that dilates poorly or not at all in response to topically administered mydriatic drugs. Dilation inability results from absent or incompletely developed dilator pupillae muscle. The sphincter pupillae muscle which acts in opposition to the dilator muscle to cause constriction of the pupil is unaltered. In addition to abnormal dilator pupillae muscle, the miotic iris is thin and it displays abnormal stroma and iridocorneal angle. [1-4] Iris thinning is consistent with transillumination of miotic irises and high sensitivity to light. High myopia and glaucoma are frequently associated with this condition.[5-8]

MCOR is a bilateral disease transmitted as an autosomal dominant trait with complete penetrance. A unique 8 Mb locus on chromosome 13q31-q32 has been mapped in 1998 by linkage analysis[9] in a large multigenerational French pedigree first described in 1964.[10] Gene mapping in some other families confirmed linkage to this locus[11] whereas some others were inconsistent with the 13q31-q32 region, supporting genetic heterogeneity of the disease. [12]

Here, we report a study combining Sanger sequencing and array comparative genomic hybridization (CGH) which allowed the identification of the molecular defect underlying the disease at the 13q31-32 locus.

We obtained DNA samples of affected and unaffected members of six MCOR families originating from France, Japan and Mexico (FR1-2, JP1-2, MX1-2, respectively). Three out of these families were previously reported (FR1, the original family which allowed mapping of the MCOR locus on chromosome 13q31-q32,[9,10] JP1[6] and MX1[4]). The pedigrees of the families are presented in Figure 1. The study was approved by Ethics committees of each participating Institutions, namely *Paris Ile-de-France II,* University of Occupational and Environmental Health, Japan and Instituto de Oftalmologia Conde de Valenciana, Mexico City. Individuals participating to the study provided informed consents for molecular analyses.

Sanger sequencing of the coding region and intron-exon boundaries of genes lying within the 8 Mb MCOR interval on 13q31-q32, and whole exome sequencing combined with linkage analysis failed to detect candidate disease-causing variants segregating with the disease in families FR1 and JP1, respectively (Table S1, Figure S1). Considering the strong linkage at the locus in FR1 (Zmax = 9.79, Θ = 0),[9] we assumed that the mutation in this family was present in an unscreened region or that it might consist in a genomic rearrangement undetectable using PCR-based screening methods. To assess this latter hypothesis, we subjected the DNA of an affected individual (FR1_III7, Figure 1) to comparative genomic hybridization (CGH) on high resolution oligonucleotide microarray (Affymetrix Cytogenetics Whole-Genome 2.7M Array). Calculation of test over reference Log2 intensity Ratios identified a 54.8 Kbp deletion in the 13q32.1 region (Figure 2, Figure S2). We amplified the junction fragment by subjecting the genomic DNA of the index case to PCR using primers designed just outside of the predicted deletion boundaries (Table S2, Figure S3). Direct sequencing of the 1.1 Kb intervening segment showed that the deletion extended from 95,227,374 to 95,277,864 (positions on

chromosome 13 according to the Genome Reference Consortium Human Build 37) with centromeric and telomeric breakpoints in intron 11 and intron 8 of the tail-to-tail genes: TDP-glucose 4,6-dehydratase *(TGDS*, NM_014305.2) and the G protein-coupled receptor 180 (*GPR180*, [NM_180989.5], also known as intimal-thickness-related receptor, *ITR* [MIM607787]), respectively (Table 1 and Figure 2).

Interestingly, multiplex PCR of short fluorescent fragments (QMPSF)[13] using primer pairs specific to *GPR180, TGDS* and a control gene *(CFTR*, NM_000492.3, Table S3) suggested hemizygosity at 13q32.1 in the other French family as well as the two Japanese and two Mexican MCOR families (Figure S4). In all five families, array CGH confirmed the presence of 13q32.1 deletions, which estimated sizes ranged from 39 Kbp to 88.9 Kbp (Figure S2). Direct sequencing of intervening segments amplified using primers designed just outside of the predicted breakpoints (Table S2) showed that the deletions extended from 95,241,606 to 95,276,905 (35.3 Kbp encompassing 4/12 *TGDS* and 7/9 *GPR180* exons), 95,228,262 to 95,300,908 (72.6 Kbp encompassing 11/12 *TGDS* exons, *GPR180* and *mir_562*), 95,236,251 to 95,309,380 (73.1 Kbp encompassing 4/12 *TGDS* exons, *GPR180 mir_562* and *5S_rRNA*) and 95,225,217 to 95,305,083 (79.9 Kbp encompassing *GPR180*, mir_562 and *5S_rRNA*) in families FR2, JP1, JP2 and MX1, respectively (Table 1, Figure 2).

In family MX2, we failed to amplify the intervening segment using primers designed with array CGH data. Considering that MX1 and MX2 families had the same ethnic background and shared the same predicted distal deletion breakpoint (Table 1 and Figure S2) we assumed that both families could have inherited the same deletion by descent and that, in corollary, lack of amplification of the junction fragment in family MX2 could result from incorrectly predicted proximal deletion breakpoint. Using the primers designed to amplify family MX1 junction fragment, we were able to amplify family MX2 intervening segment (Figure S3). Direct sequencing demonstrated the two families shared the exact same deletion (Table 1 and Figure 2). Analysis of microsatellite markers of chromosome 13q31-q32 showed that the deletion was carried by a common 6.4 Mb haplotype suggesting that it might have been transmitted within both families by a common ancestor (Figure S5).

Deletion fragment-specific PCR assays based on the amplification of intervening segments in all available DNA samples (see Figure 1) allowed us to confirm the co-segregation of the deletions with the disease in 4/6 families (Figure S3). Segregation analysis could not be performed in Families FR2 and JP2 because of a lack of DNA samples. Positive PCR amplification of intragenic *GPR180* fragments confirmed heterozygosity of all deletions (not shown).

The copy number variations identified in this study are publicly available in the DECIPHER database as 301464, 301465, 301468, 301469, 301471 and 301472. None of them have been previously reported in the DECIPHER database, the Database of Genomic Variants (DGV) or in the cohort of individuals affected with variable diseases analyzed by array CGH at our Institute (n = 96; unpublished data). However, chromosome 13q deletions are not uncommon and cause a wide spectrum of phenotypes correlated to the size and position of the deleted region. To our knowledge, microcoria has not been described in individuals with 13q deletions encompassing the 13q32.1 region. However,

microcoria could be overlooked or could not manifest owing to severe eye dysgenesis since about one third of children with 13q deletion syndrome have iris and choroid coloboma, glaucoma, cataracts, and cloudy lenses. Together, these data are consistent with the causality of 13q32.1 deletions in MCOR.

Inspection of sequences surrounding MCOR deletion breakpoints identified a duplicated sequence prone to recurrent nonallelic homologous recombination (NAHR) in a unique family (FR2, 37bp sequence shared between *TGDS* intron 4 and *GPR180* intron 7 at positions 95,241,662-95,241,698 and 95,276,905-95,276,998, respectively; Figure S6).

Recently, several microhomology-mediated repair mechanisms have been described in the etiology of non-recurrent CNVs in human disease.[14-16] These mechanisms, which are guided by the surrounding genomic architecture, include microhomology-mediated end-joining (MMEJ),[17] fork stalling and template switching (FoSTeS),[18] microhomology-mediated break-induced replication (MMBIR),[19] serial replication slippage (SRS),[20] and break-induced SRS (BISRS).[21] Extensive bioinformatic analysis of MCOR deletion breakpoints and surrounding genomic architecture allowed the identification of perfectly matching 1 or 2 base pairs shared between the proximal and distal sequence at the junctions, sequence motifs and/or repetitive elements which are likely to stimulate the formation of the 13q32.1 deletions by increasing susceptibility of DNA breakage or promote replication fork stalling (Table S4, Figures S6-7). These findings are consistent with the view that microhomology-mediated mechanisms underlie non-recurrent MCOR deletions in families FR1, JP1, JP2, MX1 and MX2.

The minimal common deletion disrupted *GPR180* and *TGDS* (Table 1 and Figure 2), raising the possibility that haploinsufficiency of one or the two genes, or alternatively the loss of regulatory elements, might give rise to the phenotype.

GPR180 encodes a 201 amino-acid G protein-coupled receptor[22] of the Rhodopsin-like receptors family which includes hormones, neurotransmitters, and light receptors, all of which transduce extracellular signals upon interaction with guanine nucleotide-binding proteins and activating ligands.[23] Very little is known about the function of GPR180. However, it has been reported to be produced predominantly in vascular smooth muscle cells where its expression is upregulated in response to experimental injury.[24] The significant suppression of DNA synthesis and inability to produce neointima in response to vascular injury in the *Gpr180*-/- mouse suggest that upregulation of *Gpr180* signaling contributes to vascular smooth muscle growth.[22] In addition, gene expression profiling in normal human tissues have shown that it is highly expressed in myoepithelia (salivary gland, endomyometrium, prostate, lung and liver).[25] In the eye, *GPR180* is less abundant than in myoepithelia. However, it is listed in the top 20 genes having a significantly higher expression in the iris compared to the other ocular structures.[26] Hence, considering that the dilator pupillae arises during embryonic life by the differentiation of iris epithelial cells into myoepithelial cells,[27,28] *GPR180* was regarded as a strong candidate MCOR gene.

The *Gpr180*-/- mouse had resistance to experimental thickening of the intima but normal appearance, growth rate, reproduction, and histology of major organs.[22] We examined *Gpr180-/- and Gpr180+/-* mice for anterior segment development and iris function. We found that both heterozygote and

homozygote *Gpr180*-null eyes were undistinguishable from adult age-matched controls (Figures S8-S10). In particular, we found no iris transillumination and normal drug-mediated mydriasis both in heterozygote and homozygote *Gpr180*-null mice.However, inspection of our in house exome database (>4200 exomes) for *GPR180* nonsense or frameshift variants with an acceptable amount of reads (≥ 10) identified a unique heterozygote *GPR180* nonsense mutation (c.343 C>T; p.Gln115*). This variant was found in our own series of individuals with neonatal retinal dystrophy, namely Leber congenital amaurosis (LCA, [MIM204000]). Interestingly, the ophthalmologic file of the blind individual harboring the p.Gln115* substitution (II2, family FR3; Figure 3) mentioned an abnormal iridocorneal angle at examination of the anterior segment of the eye. The individual, her parents and siblings consented to ophthalmological examination and genetic analysis. Iridocorneal angle dysgenesis was evidenced in all family members but the mother and a brother affected with LCA (family FR3; Figure 3). Evidence of father-to-son transmission demonstrated autosomal dominant transmission of the iridocorneal defect which segregated with the p.Gln115* substitution, independently from the autosomal recessive retinal disease (Figure 3). Whole-genome SNP genotyping data generated using Affymetrix GeneChip Human Mapping 10K 2.0 Arrays were available in this family. Retrospective analysis for linkage with the autosomal dominant anterior segment dysgenesis pointed 15 candidate chromosomal regions, including a region on 13q32.1 containing *GPR180* (Figure S11). Retrospective analysis of exome data found no heterozygote loss-of-function variants in any of these regions other than the *GRP180* p.Gln115* substitution, supporting the role of *GPR180* in the development of the irido-corneal angle. Nevertheless, none of the five individuals with both iridocorneal angle dysgenesis and the p.Gln115* substitution had abnormal pupillary response or iris transillumination. Considering that iridocorneal angle dysgenesis is a constant symptom in congenital microcoria linked to 13q32.1 (31/31, 5/5, 1/1, 2/2 and 3/3 of examined MCOR individuals in families FR1[5,9], JP1[6], JP2, MX1 and MX2, respectively; Figures 1 and 3), goniodysgenesis in family FR3 may be regarded as a MCOR endophenotype.

The reason why heterozygosity for the p.Gln115* substitution was not sufficient to cause the full range of MCOR symptoms could reside in the production of a truncated protein retaining some of its function. Alternatively, premature termination codon (PTC) self-correcting mechanisms could be involved, in particular translational read-through which has recently been reported to be more abundant than expected in higher species, including human.[29] Nonsense-associated altered splicing (NAS), which consists in selective exclusion of an in-frame exon with a premature termination codon, is another possible correcting mechanism. [30–33] Recently, a nonsense mutation in *CEP290* which mutations cause blindness has been shown to induce exon skipping and to lead to a relatively mild retinal phenotype.[34] Because the skipping of *GPR180* exon 2 would not disrupt the open reading frame, NAS could explain why the p.Gln115* substitution is not as detrimental as gene ablation.

The p.Gln115* substitution was not reported in the Exome Aggregator database (ExAC), Exome Variant Server (EVS), 1000Genome and dbSNP datasets. However, we identified in the ExAC database twelve other rare variants which may cause protein truncation (6 nonsense and 6 frameshift mutations, 0.00004 <minor allele frequency <0.000008; Table S5). Provided that these variants are confirmed, studying their molecular consequence at the mRNA and/or the protein levels and, knowing

the ophthalmologic status of carrier individuals will certainly help in understanding the role of *GPR180* in MCOR and goniodysgenesis. Meanwhile, to address this important question, we screened the *GPR180* exome for mutations in a series of individuals having an eye disease with goniodysgenesis, including ten individuals with Axenfeld-Rieger anomaly or Peters anomaly [MIM604229] and no *PAX6, PITX2, FOXC1, CYP1B1, MAF* or *MYOC* mutation (n = 5 and n = 5, respectively), and eleven index cases of primary congenital glaucoma (n = 9) or juvenile glaucoma (n = 2) with no *CYP1B1* mutations. Primer sequences are given in Table S6. No *GPR180* candidate disease variants were identified in *GPR180* exon and intron-exon boundaries in any of the individuals.

Despite strong arguments in favor of the involvement of GPR180 in MCOR, in the absence of 13q32.1 deletions which do not disrupt *TGDS,* or of a *GPR180* mutation that causes the full MCOR phenotype, we cannot formally exclude that haploinsufficiency of *GPR180* is necessary, but not sufficient, for MCOR to manifest.

The second gene lost or disrupted in MCOR individuals, *TGDS,* encodes the dTDP-D-glucose 4,6-dehydratase, an evolutionarily conserved NAD-dependent sugar epimerase/dehydratase of the short chain dehydrogenase/reductase extended-type family (SDR2E1, EC:4.2.1.46). In human, SDR enzymes display a wide substrate spectrum, ranging from steroids, alcohols, sugars, and aromatic compounds to xenobiotics.[35] TGDS catalyses the dehydration of dTDP-alpha-D-glucose into dTDP-4-dehydro-6-deoxy-alpha-D-glucose. It contributes to deoxy-sugar metabolism,[35,36] but its exact function is unknown. In bacteria, TGDS is essential to the biogenesis of cell envelope components and antibiotics,[37] while in *C. elegans*, it is required for normal growth rates, larval development and survival, reproduction and coordinated locomotion.[38] In human eyes, *TGDS* expression is lower than that of *GPR180*, and unlike this latter, it has no preferential expression in the iris[26]. More importantly,very recently, biallelic *TGDS* mutations have been reported to cause Catel-Manzke syndrome [MIM302380] which is characterized by Pierre Robin sequence (MIM 261800; HP:0000201) and a unique form of bilateral hyperphalangy causing clinodactyly of the index finger (HP:0009467).[39] Neither the affected individuals, nor their heterozygote parents are reported to have eye disease.[39]Therefore, it is unlikely that TGDS dysfunction in human is responsible for MCOR.

Finally, it cannot be excluded that full range of MCOR symptoms are due to both the loss of GPR180 function and to that of elements that regulate the expression of neighboring genes by position effect. Inspection of the ENCODE repository for transcription factor-binding site identified by CHIPseq detected no eye-specific binding sites in the 35.3 Kbp sequence of the shortest MCOR deletion (Figure S12). Likewise, inspection of the database of conserved non-coding orthologous regions (CONDOR) identified no highly conserved non-coding elements (HCNE) in the 35.3 Kbp MCOR minimal region. However, two genes involved in eye development are located close to the MCOR region, namely *DCT* [MIM191275] which encodes the dopachrome tautomerase and *SOX21* [MIM604974] which encodes SRY-related high-mobility-group box 21.

DCT is located 110 Kbp upstream of proximal boundary of the minimal interval (Figure 2). It functions downstream of tyrosinase (TYR) [MIM606933] and tyrosinase-related protein-1 (TRP1) [MIM115501)

in the biosynthetic pathway of eumelanin in pigment cells. In the mouse, *Dct* mutations cause the Slaty phenotype in which the iris is normal in the first months of life. Later-on, age-related dispersed pigment across the surface of the iris combined with mild transillumination is noted[40]. To our knowledge, no *DCT* mutation is reported in human disease so far but 10 loss-of-function alleles are described in EVS. One of these variants, p.Tyr75Serfs*50 is homozygous in 12/6249 individuals, making unlikely a contribution of DCT loss-of-function in MCOR. However, considering that pigmentation has a role on the development of the neuroretina,[41,42] it cannot be excluded that 13q32.1 deletions cause *DTC* overexpression and dysregulate iris development mechanisms.

SOX21 is located 75 kbp upstream of the distal boundary of the minimal MCOR interval (Figure 2). Sox21 has been reported to be a general mediator of the effects of Sox2[43] which interaction with Pax6 is crucial to coordinate eye development[44]. It is known to be expressed in the developing lens in chicken[45] and zebrafish.[46] Additionally, *sox21*b knock-down in the zebrafish causes lens malformation.[47] In the mouse, complete inactivation of *Sox21* has been reported to cause cyclic alopecia,[48] but the ocular phenotype of the animal is unknown. Altered regulation of *SOX21* expression in MCOR individuals cannot be excluded.

In summary, here we report heterozygote 13q32.1 deletions in 6/6 MCOR families of variable ethnic origin, which invariably encompass *GPR180* and *TGDS.* We suggest that *GPR180* ablation, alone or in combination with the loss of elements that regulate the expression of neighboring genes by position effect, is the cause of the disease. Further studies will hopefully allow the identification of the molecular mechanisms underlying this rare disease. It should provide further insights into the development of the anterior chamber of the eye, which anomalies are an important cause of visual loss due to glaucoma.

Supplemental data

Figures S1-S12; Table S1-S6

Acknowledgments

We are grateful to the families for their participation in the study. We thank Johan Castille and Gérard Pivert for technical assistance. This work was supported by grants from the Fédération des Aveugles de France (FAF) to LFT, Retina France to JMR and Geniris to JMR and PC, the Ministry of Education, Culture, Sport, Science and Technology of Japan Grant-in-aid N°20592067 to AT and the Conde de Valenciana Foundation patronage to ARM and JCZ. None of the authors of this manuscript have a financial interest related to this work.

Web Resources

The URLs for data presented herein are as follows:

1000 Genomes, http://www.1000genomes.org

The database of conserved non-coding orthologous regions, http://condor.nimr.mrc.ac.uk/

Database of Genomic Variants (DGV), http://dgv.tcag.ca/dgv/app/home

dbSNP, http://www.ncbi.nlm.nih.gov/SNP/

Decipher, https://decipher.sanger.ac.uk/

Exome Aggregator database, http://exac.broadinstitute.org/

Exome Variant Server (EVS), http://evs.gs.washington.edu/EVS

Genome browser, http://genome.ucsc.edu

Online Mendelian Inheritance in Man (OMIM), http://www.omim.org

NCBI Reference Sequence Database, http://www.ncbi.nlm.nih.gov/refseq/Refseq

UCSC Genome Browser, http://genome.ucsc.edu

Accession Numbers

The accession number for the copy number variants in the DECIPHER database are 301464, 301465, 301468, 301469, 301471 and 301472.

References

1. Butler JM, Raviola G, Miller CD, Friedmann AI (1989). Fine structural defects in a case of congenital microcoria. Graefes Arch Clin Exp Ophthalmol. 227:88-94.

2. Simpson WA, Parsons MA (1989). The ultrastructural pathological features of congenital microcoria. A case report. Arch Ophthalmol. 107:99-102.

3. Pietropaolo A, Corvino C, DeBlasi A, Calabrò F (1998). Congenital microcoria: case report and histological study. J Pediatr Ophthalmol Strabismus. 35:125-7.

4. Ramirez-Miranda A, Paulin-Huerta JM, Chavez-Mondragón E, Islas-de la Vega G, Rodriguez-Reyes A (2011). Ultrabiomicroscopic-histopathologic correlations in individuals with autosomal dominant congenital microcoria: three-generation family report. Case Rep Ophthalmol. 2:160-5.

5. Toulemont PJ, Urvoy M, Coscas G, Lecallonnec A, Cuvilliers AF (1995). Association of congenital microcoria with myopia and glaucoma. A study of 23 patients with congenital microcoria. Ophthalmology. 102:193-8.

6. Tawara A, Itou K, Kubota T, Harada Y, Tou N, Hirose N (2005). Congenital microcoria associated with late-onset developmental glaucoma. J Glaucoma 14:409-13.

7. Mazzeo V, Gaiba G, Rossi A (1986). Hereditary cases of congenital microcoria and goniodysgenesis. Ophthalmic Paediatr Genet. 7:121-5.

8. Tawara A, Inomata H (1983). Familial cases of congenital microcoria associated with late onset congenital glaucoma and goniodysgenesis. Jpn J Ophthalmol. 27:63-72.

9. Rouillac C, Roche O, Marchant D, Bachner L, Kobetz A, Toulemont PJ, Orssaud C, Urvoy M, Odent S, Le Marec B, Abitbol M, Dufier JL (1998). Mapping of a congenital microcoria locus to 13q31-q32. Am J Hum Genet. 62:1117-22.

10. Ardouin M, Urvoy M, Lefranc J. Microcorie congénitale (1964). Bulletins et Mémoires de la Société Française d'Ophtalmologie 77:356–63. 4.

11. Ramprasad VL, Sripriya S, Ronnie G, Nancarrow D, Saxena S, Hemamalini A, Kumar D, Vijaya L, Kumaramanickavel G (2005). Genetic homogeneity for inherited congenital microcoria loci in an Asian Indian pedigree. Mol Vis. 11:934-40.

12. Bremner FD, Houlden H, Smith SE (2004). Genotypic and phenotypic heterogeneity in familial microcoria. Br J Ophthalmol. 88:469-73.

13. Saugier-Veber P, Goldenberg A, Drouin-Garraud V, de La Rochebrochard C, Layet V, Drouot N, Le Meur N, Gilbert-Du-Ssardier B, Joly-Hélas G, Moirot H, Rossi A, Tosi M, Frébourg T (2006). Simple detection of genomic microdeletions and microduplications using QMPSF in patients with idiopathic mental retardation. Eur J Hum Genet. 14:1009-17.

14. Stankiewicz P., Lupski J.R (2002). Genome architecture, rearrangements and genomic disorders. Trends Genet. 18:74–82.

15. Vissers LE, Bhatt SS, Janssen IM, Xia Z, Lalani SR, Pfundt R, Derwinska K, de Vries BB, Gilissen C, Hoischen A, Nesteruk M, Wisniowiecka-Kowalnik B, Smyk M, Brunner HG, Cheung SW, van Kessel AG, Veltman JA, Stankiewicz P (2009). Rare pathogenic microdeletions and tandem duplications are microhomology-mediated and stimulated by local genomic architecture. Hum Mol Genet. 18:3579-93.

16. Verdin H, D'haene B, Beysen D, Novikova Y, Menten B, Sante T, Lapunzina P, Nevado J, Carvalho CM, Lupski JR, De Baere E. Microhomology-mediated mechanisms underlie non-recurrent disease-causing microdeletions of the FOXL2 gene or its regulatory domain (2013). PLoS Genet. 9:e1003358.15.

17. Lieber M.R (2008). The mechanism of human nonhomologous DNA end joining. J. Biol. Chem. 283:1-5.

18. Lee J.A., Carvalho C.M., Lupski J.R (2007). A DNA replication mechanism for generating nonrecurrent rearrangements associated with genomic disorders. Cell. 131:1235-1247.

19. Hastings PJ, Ira G, Lupski JR (2009). A microhomology-mediated break-induced replication model for the origin of human copy number variation. PLoS Genet. 5:e1000327.

20. Chen JM, Chuzhanova N, Stenson PD, Ferec C, Cooper DN (2005) Complex gene rearrangements caused by serial replication slippage. Hum Mutat. 26:125-34.

21. Sheen CR, Jewell UR, Morris CM, Brennan SO, Ferec C, et al. (2007) Double complex mutations involving F8 and FUNDC2 caused by distinct break-induced replication. Hum Mutat. 28:1198-206.

22. Tsukada S, Iwai M, Nishiu J, Itoh M, Tomoike H, Horiuchi M, Nakamura Y, Tanaka T (2003). Inhibition of experimental intimal thickening in mice lacking a novel G-protein-coupled receptor. Circulation. 107:313-9.

23. G Milligan (2008). A day in the life of a G protein-coupled receptor: the contribution to function of G protein-coupled receptor dimerization. Br J Pharmacol. 153(Suppl 1): S216–S229.

24. Iida A, Tanaka T, Nakamura Y (2003). High-density SNP map of human ITR, a gene associated with vascular remodeling. J Hum Genet. 48:170-2.

25. Shyamsundar R, Kim YH, Higgins JP, Montgomery K, Jorden M, Sethuraman A, van de Rijn M, Botstein D, Brown PO, Pollack JR (2005). A DNA microarray survey of gene expression in normal human tissues. Genome Biol. 6:R22.

26. Wagner AH, Anand VN, Wang WH, Chatterton JE, Sun D, Shepard AR, Jacobson N, Pang IH, Deluca AP, Casavant TL, Scheetz TE, Mullins RF, Braun TA, Clark AF (2013). Exon-level expression profiling of ocular tissues. Exp Eye Res. 111:105-11.

27. Lai YL (1972). The development of the dilator muscle in the iris of the albino rat. Exp Eye Res. 14:203-7.

28. Lai YL (1972).The development of the sphincter muscle in the iris of the albino rat. Exp Eye Res. 14:196-202.

29. Jungreis I, Lin MF, Spokony R, Chan CS, Negre N, Victorsen A, White KP, Kellis M (2011). Evidence of abundant stop codon readthrough in Drosophila and other metazoa. Genome Res. 21:2096-113.

30. Dietz HC, Valle D, Francomano CA, Kendzior RJ Jr., Pyeritz RE, Cutting GR (1993). The skipping of constitutive exons in vivo induced by nonsense mutations. Science. 259:680–683.

31. Valentine CR (1998). The association of nonsense codons with exon skipping. Mutat Res. 411:87–117.

32. Cartegni L, Chew SL, Krainer AR (2002). Listening to silence and understanding nonsense: exonic mutations that affect splicing. Nat Rev Genet. 3:285–298.

33. Wang J, Chang YF, Hamilton JI, Wilkinson MF (2002). Nonsense-associated altered splicing: a frame-dependent response distinct from nonsense-mediated decay. Mol Cell. 10:951–957.

34. Littink KW, Pott JW, Collin RW, Kroes HY, Verheij JB, Blokland EA, de Castro Miró M, Hoyng CB, Klaver CC, Koenekoop RK, Rohrschneider K, Cremers FP, van den Born LI, den Hollander AI (2010). A novel nonsense mutation in CEP290 induces exon skipping and leads to a relatively mild retinal phenotype. Invest Ophthalmol Vis Sci. 51:3646-52.

35. Kallberg Y, Oppermann U, Jörnvall H, Persson B (2002). Short-chain dehydrogenase/reductase (SDR) relationships: a large family with eight clusters common to human, animal, and plant genomes. Protein Sci. 11:636-41.

36. Persson B, Kallberg Y, Bray JE, Bruford E, Dellaporta SL, Favia AD, Duarte RG, Jörnvall H, Kavanagh KL, Kedishvili N, Kisiela M, Maser E, Mindnich R, Orchard S, Penning TM, Thornton JM, Adamski J, Oppermann U (2009). The SDR (short-chain dehydrogenase/reductase and related enzymes) nomenclature initiative. Chem Biol Interact. 178:94-8.

37. Allard STM, Beis K, Giraud MF, Hegeman AD, Gross JW, Wilmouth RC, Whitfield C, Graninger M, Messner P, Allen AG, Maskell DJ, Naismith JH (2002). "Toward a structural understanding of the dehydratase mechanism". Structure. 10: 81–92.

38. Levin M, Hashimshony T, Wagner F, Yanai I (2012). Developmental milestones punctuate gene expression in the Caenorhabditis embryo. Dev Cell. 22:1101-8.

39. Ehmke N, Caliebe A, Koenig R, Kant SG, Stark Z, Cormier-Daire V, Wieczorek D Gillessen-Kaesbach G,9 Hoff K, Kawalia A Thiele H, Altmüller J, Fischer-Zirnsak B, Knaus A, Zhu N, Heinrich V, Huber C, Harabula I Spielmann M,Horn D, Kornak U, Hecht J, Krawitz PM,Nürnberg P, Siebert R, Manzke H, Mundlos S (2014). Homozygous and compound-heterozygous mutations in TGDS cause Catel-Manzke syndrome. Am J Hum Genet. 95:763-70.

40. Anderson MG1, Hawes NL, Trantow CM, Chang B, John SW (2008). Iris phenotypes and pigment dispersion caused by genes influencing pigmentation. Pigment Cell Melanoma Res. 21:565-78.

41. Grønskov K, Ek J, Brondum-Nielsen K (2007). Oculocutaneous albinism. Orphanet J Rare Dis. 2:43. Review.

42. Bhansali P, Rayport I, Rebsam A, Mason C (2014). Delayed neurogenesis leads to altered specification of ventrotemporal retinal ganglion cells in albino mice. Neural Dev. 9:11.

43. Kuzmichev AN, Kim SK, D'Alessio AC, Chenoweth JG, Wittko IM, Campanati L, McKay RD (2012). Sox2 acts through Sox21 to regulate transcription in pluripotent and differentiated cells. Curr Biol. 22:1705-10.

44. Matsushima D, Heavner W, Pevny LH (2011). Combinatorial regulation of optic cup progenitor cell fate by SOX2 and PAX6. Development. 138: 443–454.

45. Uchikawa M, Kamachi Y, Kondoh H (1999). Two distinct subgroups of Group B Sox genes for transcriptional activators and repressors: their expression during embryonic organogenesis of the chicken. Mech Dev. 84:103-20.

46. Lan X, Wen L, Li K, Liu X, Luo B, Chen F, Xie D, Kung HF (2011). Comparative analysis of duplicated sox21 genes in zebrafish. Dev Growth Differ. 53:347-56.

47. Pauls S, Smith SF, Elgar G (2012). Lens development depends on a pair of highly conserved Sox21 regulatory elements. Dev Biol. 365:310-8.

48. Kiso M, Tanaka S, Saba R, Matsuda S, Shimizu A, Ohyama M, Okano HJ, Shiroishi T, Okano H, Saga Y (2009). The disruption of Sox21-mediated hair shaft cuticle differentiation causes cyclic alopecia in mice. Proc Natl Acad Sci U S A. 106:9292-7.

Legends to tables and figures

Table 1. Summary of 13q32.1 deletions identified by array CGH and characterized by sequencing of the intervening segments. †denotes a partial deletion of the gene (see Figure S2). Sequences shared between the proximal and distal sequences at the junction are underlined. The breakpoint (/) has been arbitrary placed at the 5' of the identical sequences. Nucleotide positions refer to the human genome reference sequence (hg19 assembly) available at UCSC (http://genome.ucsc.edu/).

Figure 1. Pedigrees of the six families segregating MCOR. Autosomal dominant transmission is supported by father to son transmission in all six families. Individual numbers in pedigrees FR1[9] and JP1[6] are those previously reported. Available DNAs can be identified by the presentation of their genotype at the 13q32.1 locus (Del: deletion, +: wildtype allele). Individuals affected with MCOR who were examined by gonioscopy (asterisk) had all iridocorneal angle dysgenesis.

Figure 2. Overview of the 13q32.1 deletions identified in MCOR. Overview of the 13q32.1 locus (chr13:95,110,000-95,375,000; hg19) with custom tracks showing the delineated deletions presented in this study (horizontal red bars). At the top, the RefSeq Genes Track is included. In addition, ENCODE and conservation tracks are displayed.

Figure 3. Pedigree, *GPR180* genotypes and gonioscopic aspects in family FR3 and FR1. The iris spicules (arrows) consistent with an abnormal development of the iridocorneal angle are seen in individuals harboring the *GPR180* c.343C>T (p.Gln115*) mutation only as well as in individual FR1_V1 affected with microcoria. MCOR: microcoria; GD: goniodysgenesis; LCA: Leber congenital amaurosis.

		Deletions predicted by Array CGH					Actual deletions			
		Centromeric boundaries		Telomeric boundaries						
Families	Individuals	+Probe (position)	-Probe (position)	-Probe (position)	+Probe (position)	Estimated size (Kbp)	Deletion breakpoints	Size (Kbp)	Genes included or disrupted by the deletion	Sequence of the junction fragment
FR1	III7	C-08UO9 95,224,547	C-08UOA 95,225,723	S-2NJCM 95,276,735	C-08UPK 95,279 ,378	54.8	95,227,374-95,277,864	50.5	*TGDS†, GPR180†*	AAAAATCAACTATTTTTTCTTCTTAACTTC TAAAGTCATTCAATACTGAACTTGGT/**AT**GC AAATATGAATGTACATTCTTTTTTCTTTTAC AGGAATATTACACATTTGTG
FR2	II1	C-3ZRLF 95,238,814	C-3DRMS 95,238,827	C-6YHLK 95,277,799	C-4AEYA 95,277,841	39.0	95,241,606-95,276,905	35.2	*TGDS†, GPR180†*	TCACCCAGGCTGGAGTGCAGTGGTGCAACCT CAGCTCACTGCAAGCTCTGTCTCCC/**GGGTT CACGCCATTCTCCTGCCTCAGCCTCCCGAGT A**ACTCGCGCCCACGCCCGGCTAAGTTTTTGT ATTTTTAGTAGAGACGGGGTTTCACCG
JP1	IV1	S-4RUHL 95,211,097	C-7G8VT 95,211,706	C-5TEUV 95,299,777	C-5TIVX 95,300,029	88.9	95,228,262-95,300,908	72.6	*TGDS†, GPR180, mir_562*	ATCATTATTTTACATACATGTAAAAAAGAAA AAAGCTACAATAATAATTATAAGACACCAGT /**G**TCCTCTCTCAGCACAGCAGTTTACTTCTT CAGGGGCAGCAGGAGAATCTCTCTGACTTC
JP2	III7	C-3ERLF 95,238,800	C-3DRMJ 95,238,827	S-4OHPW 95,309,706	C-6MYDV 95,309,751	70.9	95,236,251-95,309,380	73.1	*TGDS†, GPR180, mir_562, 5S_rRNA*	CGATGATCAATGTCACTTACAGTAAGAAAAA CCCAAATTAAAAACTCAGAGATAC/TCTCAT TCTCCAGCTGAAATTCTCAGAAATAATGTCT ATGCCATGTACTTTCCCC
MX1	II3	S-3HRGB 95,218,014	C-6DQEK 95,219,578	C-6IBIF 95,305,254	C-4DJSK 95,305,294	87.2	95,225,217-95,305,083	79.9	*TGDS, GPR180, mir_562, 5S_rRNA*	AACCAACTGAAAGGAGAAAAAAAGTTGATCT TAGTTTATAGATGGATTGGCCTGTTC/**TG**AG CCCCATAACAGTGAGCACCTCTAGCACCTAG GATGCCAGCTGCATGTAT
MX2	III1	C-7ALKO 95,227,834	C-3GDLS 95,227,835	C-6IBIF 95,305,254	C-4DJSK 95,305,294	77.5	95,225,217-95,305,083	79.9	*TGDS, GPR180, mir_562, 5S_rRNA*	AACCAACTGAAAGGAGAAAAAAAGTTGATCT TAGTTTATAGATGGATTGGCCTGTTC/**TG**AG CCCCATAACAGTGAGCACCTCTAGCACCTAG GATGCCAGCTGCATGTAT

Table 1.

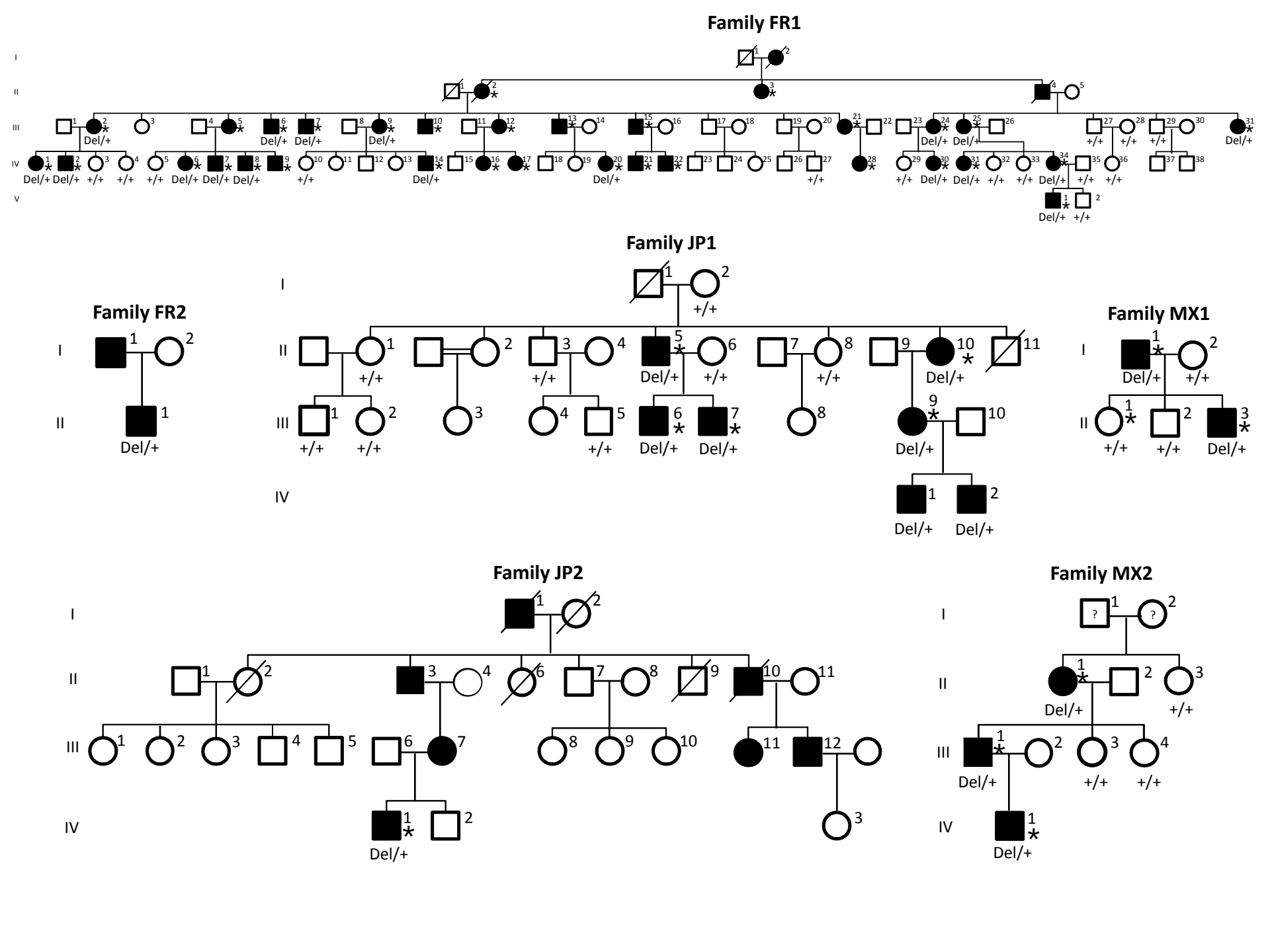
Family FR1
Family JP1
Family FR2
Family MX1
Family JP2
Family MX2
Del/+
+/+
?


chr13 (q32.1)
p13
13p12
13p11.2
12.3
q13.3
q14.11
14.2
q14.3
q21.1
21.33
13q31.1
q31.3
32.1
33.3
13q34
100 kb
hg19
95,150,000
95,200,000
95,250,000
95,300,000
95,350,000
RefSeq Genes
DCT
TGDS
GPR180
mir_562
5S-rRNA
LOC101927248
SOX21
SOX21-AS1
FR1
FR2
JP1
JP2
MX1
MX2
H3K27Ac Mark (Often Found Near Active Regulatory Elements) on 7 cell lines from ENCODE
Digital DNaseI Hypersensitivity Clusters in 125 cell types from ENCODE
Transcription Factor ChIP-seq (161 factors) from ENCODE with Factorbook Motifs
4.88
100 vertebrates Basewise Conservation by PhyloP
-4.5
Multiz Alignments of 100 Vertebrates
Rhesus
Mouse
Dog
Elephant
Chicken
X_tropicalis
Zebrafish
Lamprey

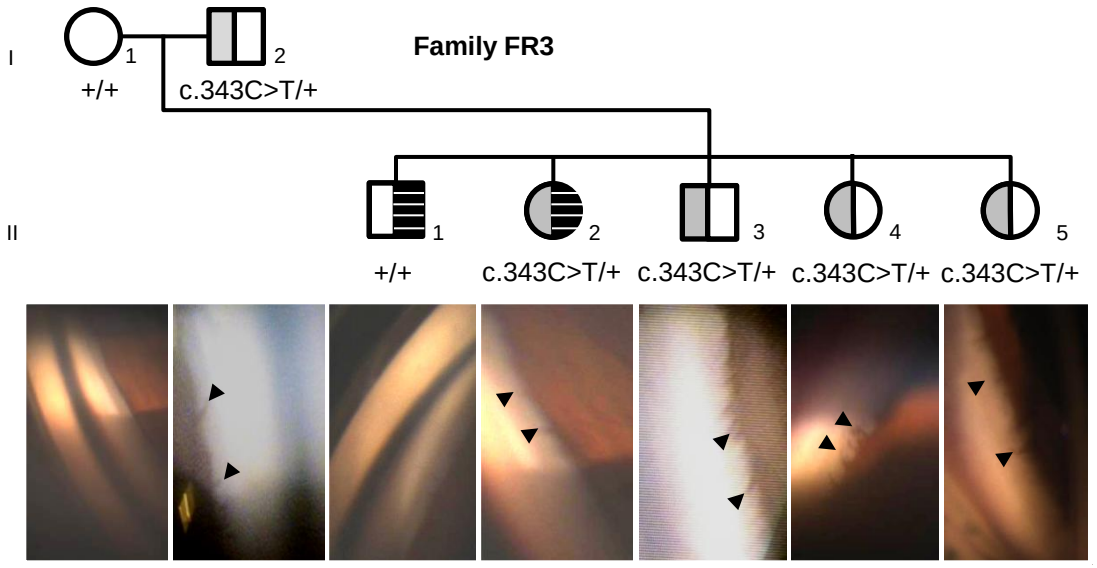
I
II
1
2
+/+
c.343C>T/+
Family FR3
1
2
3
4
5
+/+
c.343C>T/+
c.343C>T/+
c.343C>T/+
c.343C>T/+

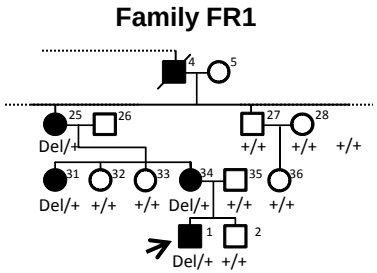
Family FR1
4
5
25
26
27
28
Del/+
+/+
+/+
+/+
31
32
33
34
35
36
Del/+
+/+
+/+
Del/+
+/+
+/+
1
2
Del/+
+/+

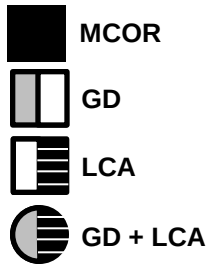
MCOR
GD
LCA
GD + LCA

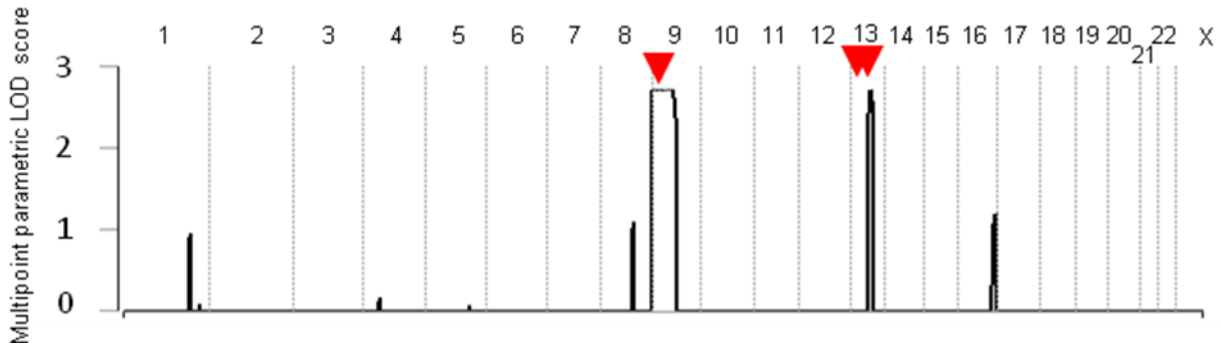

Figure S1. Multipoint parametric LOD scores in family JP1. Genome wide scan for mapping was performed using Illumina OminiExpress array (Illumina, Sandiego, CA, USA). All SNP markers were tested for Mendelian error prior to linkage analysis to exclude them from further analysis, and a set of markers were selected from the rest of the markers by the easyLINKAGE Plus program (v5.08). Multipoint parametric linkage analysis was performed by GeneHunter v2.1r5 program with an estimation of the disease allele frequency of 0.001 and a penetrance of 100% in a dominant model. Three candidate regions were compatible with linkage: chr9:1-85756778, chr13:47380943-60466889, and ch13:75085467-100692439.

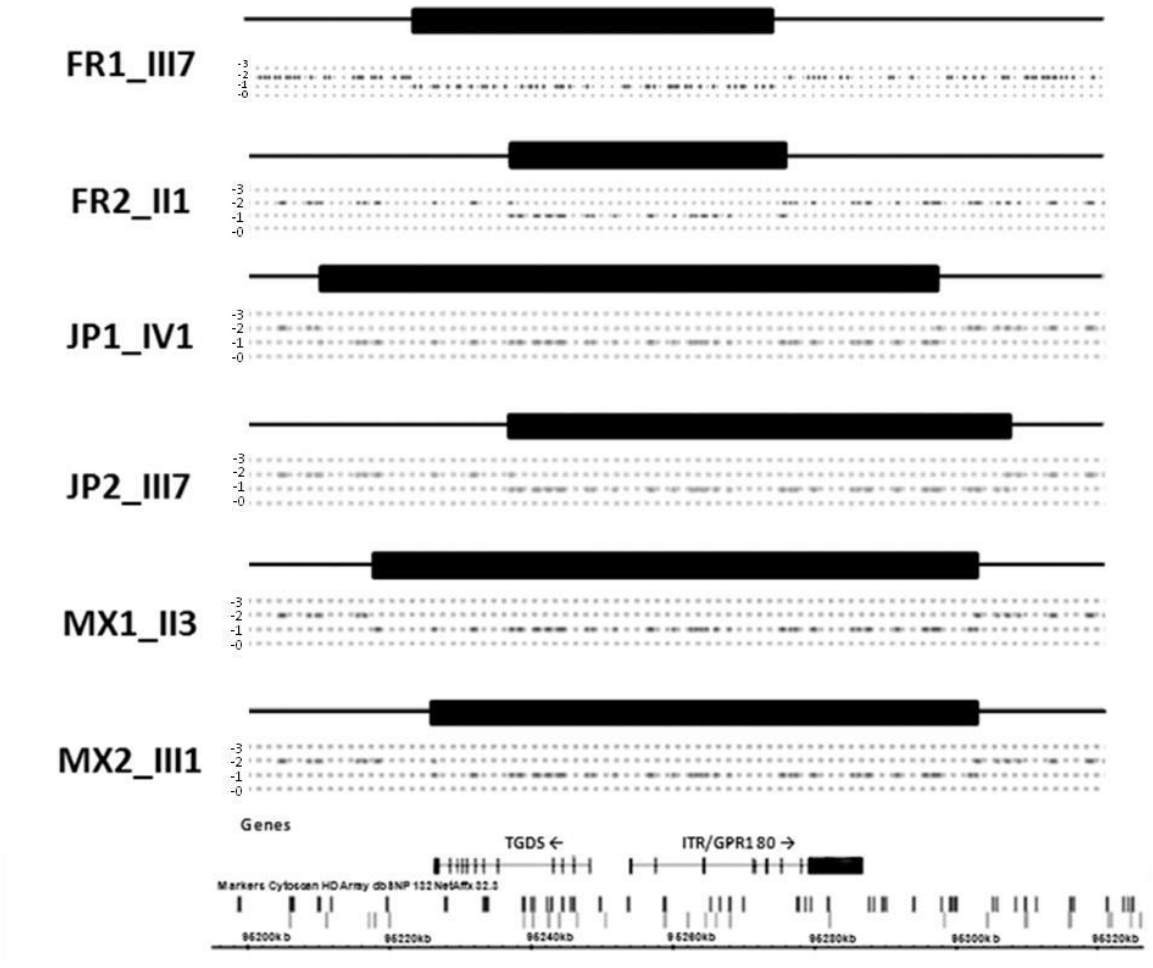

Figure S2. Copy Number state on chromosome 13q32.1, determined by comparative genomic hybridization (CGH). Genomic DNAs (250 ng) were amplified, fragmented, labeled with biotin, and hybridized onto a Whole-Genome Cytogenetics 2.7M Array (individual FR1_III7) or CytoScan® HD Arrays (individuals FR2_II1, JP1_IV1, JP2_III7, MX1_II3, MX2_III1) as recommended by the manufacturer (Affymetrix, High Wycombe, United Kingdom). After scanning, the images of the chips (.dat files) were converted into .cel files using Command Console (version 3.2). The .cel files were analyzed for Copy Number variations and loss of heterozygosity (LOH) detection. The results obtained were visualized using Chromosome Analysis Suite version 2.0.0.195 with NetAffx Build 32.3 (hg19) annotations and reference files (Affymetrix). Array CGH analysis identifies five different heterozygote deletions invariably encompassing *TGDS* and *GPR180*.

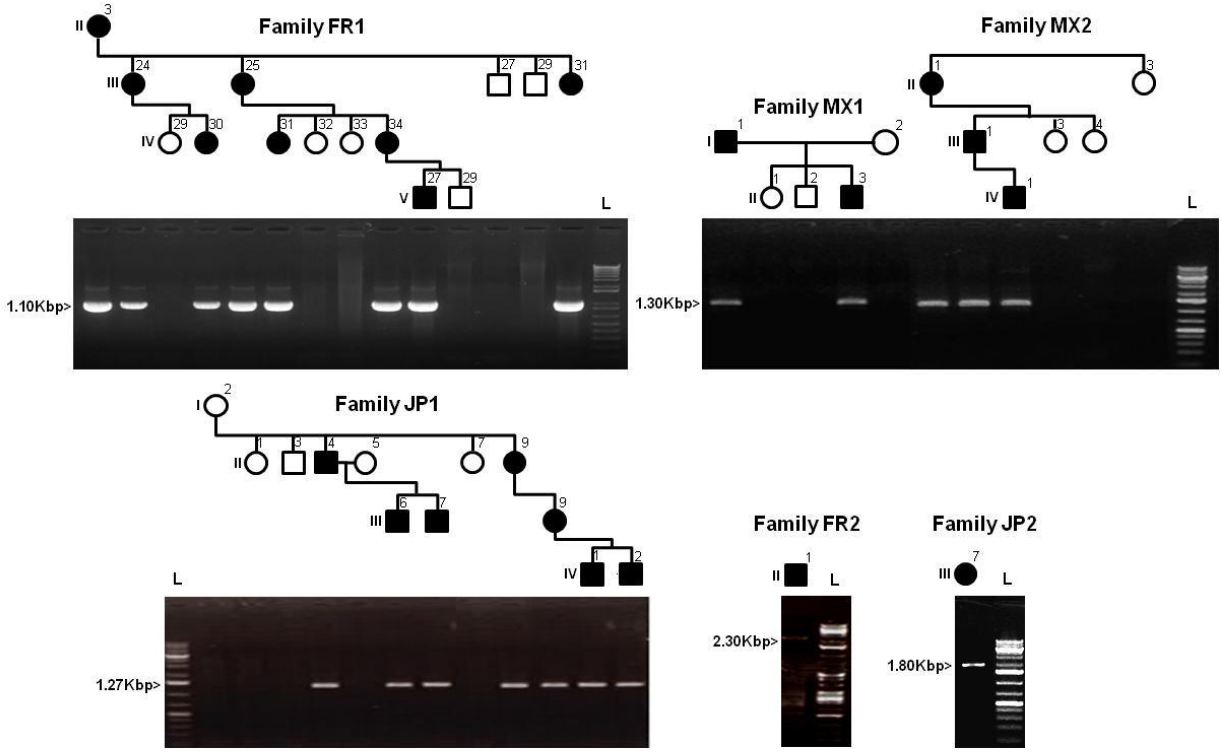

Figure S3. PCR amplification of intervening segments and segregation analysis of 13q32.1 deletions in MCOR families. The genomic DNA from affected and unaffected individuals were subjected to PCR amplification using primers designed just outside of the deletion breakpoints. The localization of the forward and reverse primers hampered amplification of the undeleted allele but not of the deleted allele, which size varied between 1.10 to 2.30 Kbp. L: 1 KbPlus DNA Ladder (Thermo Scientific). Positive and negative PCR amplifications in affected and unaffected individuals support cosegregation of the 13q32.1 deletions and the disease in 4/6 MCOR families (FR1, JP1, MX1 and MX2). All available samples of family FR1 (see Figure 1) were analyzed, but only a representative selection is shown. With respect to families FR2 and JP2, positive PCR amplifications are observed for individual II1 and III7 but no other DNAs were available.

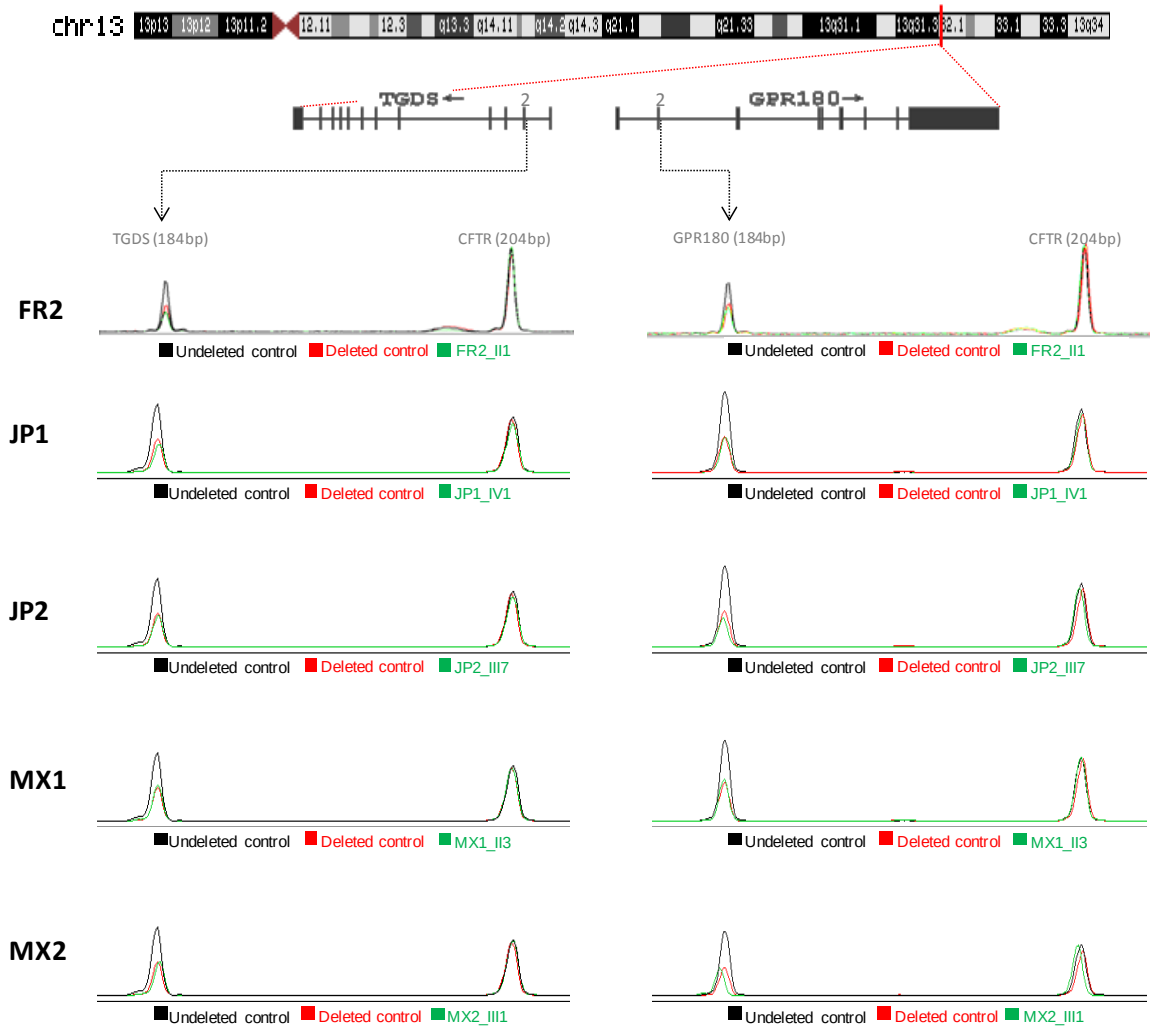

Figure S4. Quantitative multiplex PCR of short fragments analysis to assess *TGDS* and *GPR180* copy numbers in MCOR individuals FR2_II1, JP1_IV1, JP2_III7, MX1_II3, MX2_III1. DNAs from affected and control individuals were subjected to a limited number of PCR cycles (n = 23) using dye-labeled (6-FAM) primers specific to *CFTR* exon 25 (204 bp) and *TGDS* exon 2 (184 bp) or *GPR180* exon 2 (184 bp). Amplified fragments were separated by electrophoresis on an automated sequencer (Applied Biosystems, Foster City, CA). Data were analyzed using the Genescan software (Applied Biosystems) and the GeneScan-500 Rox as the ladder (Applied Biosystems). To determine *TGDS* and *GPR180* copy numbers in affected individuals, the height of *CFTR* electrophoregrams were superimposed and adjusted to those generated from control DNAs and the heights of the corresponding peaks were then compared between the different samples. The 0.5 reduction of *TGDS* and *GPR180* peak heights for individuals FR2_II1, JP1_IV1, JP2_III7, MX1_II3, MX2_III1 and FR1_III7 (deleted control) compared to FR1_V2 (undeleted control) support hemizygosity of exon 2 in both genes.

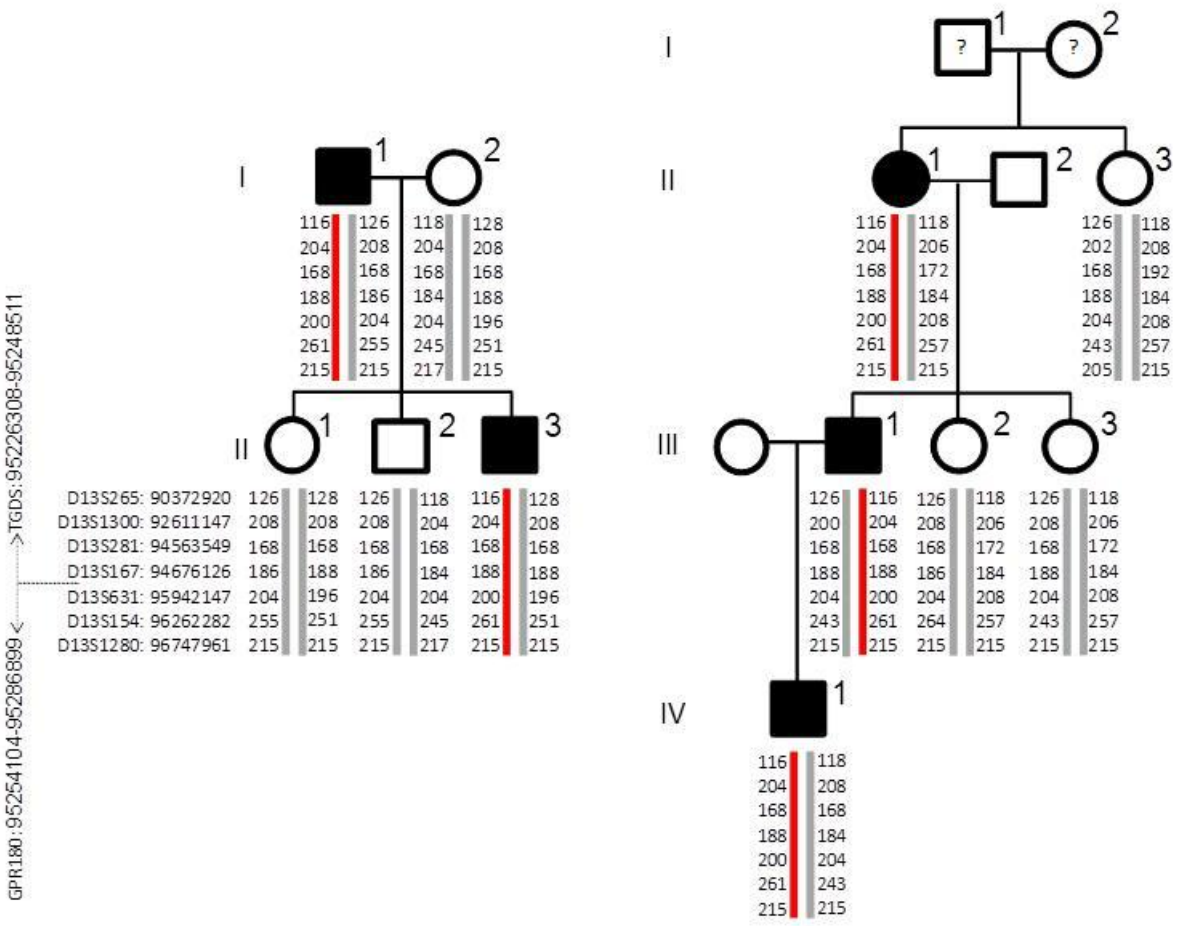

Figure S5. Haplotype analysis at the 13q31-q32 locus in the two MCOR Mexican families (MX1, MX2). Affected individuals of the two families share the same disease haplotype (in red) supporting founder effect. Chromosomal positions of microsatellite markers are indicated in base pairs according to the hg19 draft of the human genome sequence available at UCSC database. ?: clinical status unknown.

Figure S6. Multiple sequence alignment of the 13q32.1 deletion junctions. Sequences of 150 bp surrounding each junction are aligned to the proximal (displayed in blue) and distal (displayed in green) reference sequences using Clustal Omega. The junction sequences are depicted in the color of the reference sequence they align with. Pink sequences depict microhomology and homology between the proximal and distal reference sequence and the junction in families FR1, JP1, JP2, MX1, MX2, and FR2, respectively.

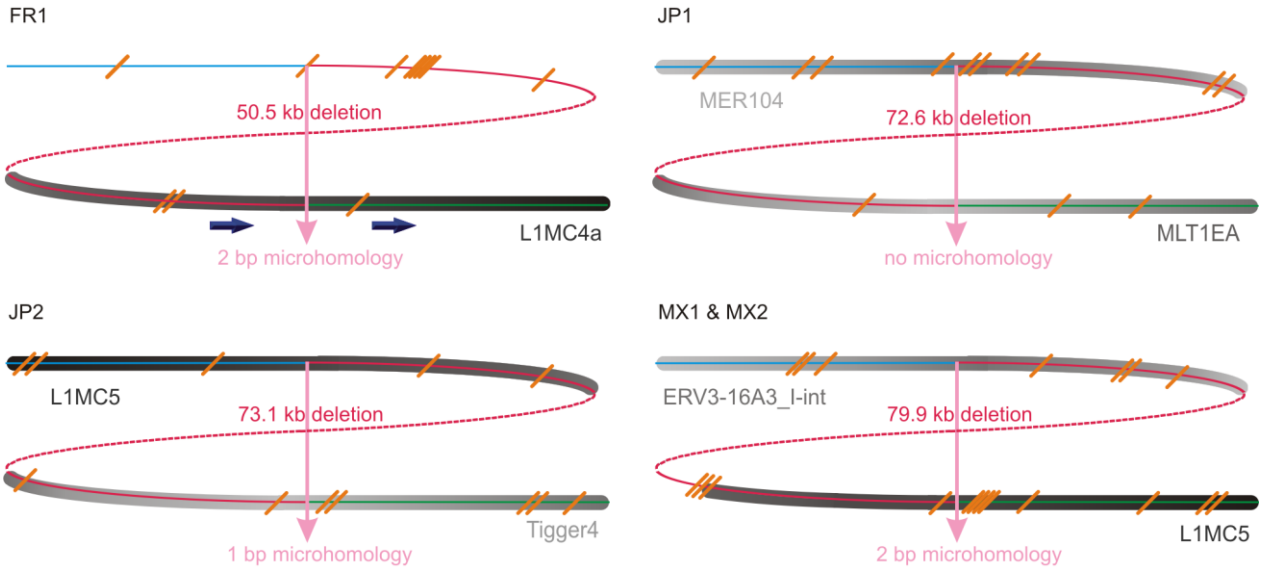

Figure S7. Schematic representations of the genomic architecture for the 13q32.1 deletions. The breakpoint regions joined by the deletion are shown. A breakpoint region is displayed as the combination of two colored, solid lines together representing a 150 bp DNA sequence. The proximal breakpoint region consists of a non-deleted blue line and a deleted red line while the distal breakpoint region consists of a deleted red line and a non-deleted green line. Each deletion is composed of the two red, solid lines joined by the red dashed line which represents the different size of the deletion for every patient. The actual size of the deletions is indicated above the red dotted lines. The pink vertical arrows mark the position of the breakpoints displaying the number of base pairs of microhomology between both breakpoint regions and the junction product. The presence of repetitive elements is shown as bars of different shades of gray. Sequence motifs are indicated with orange, skewed lines intersecting with the sequence. Direct repeats are represented by dark purple arrows.

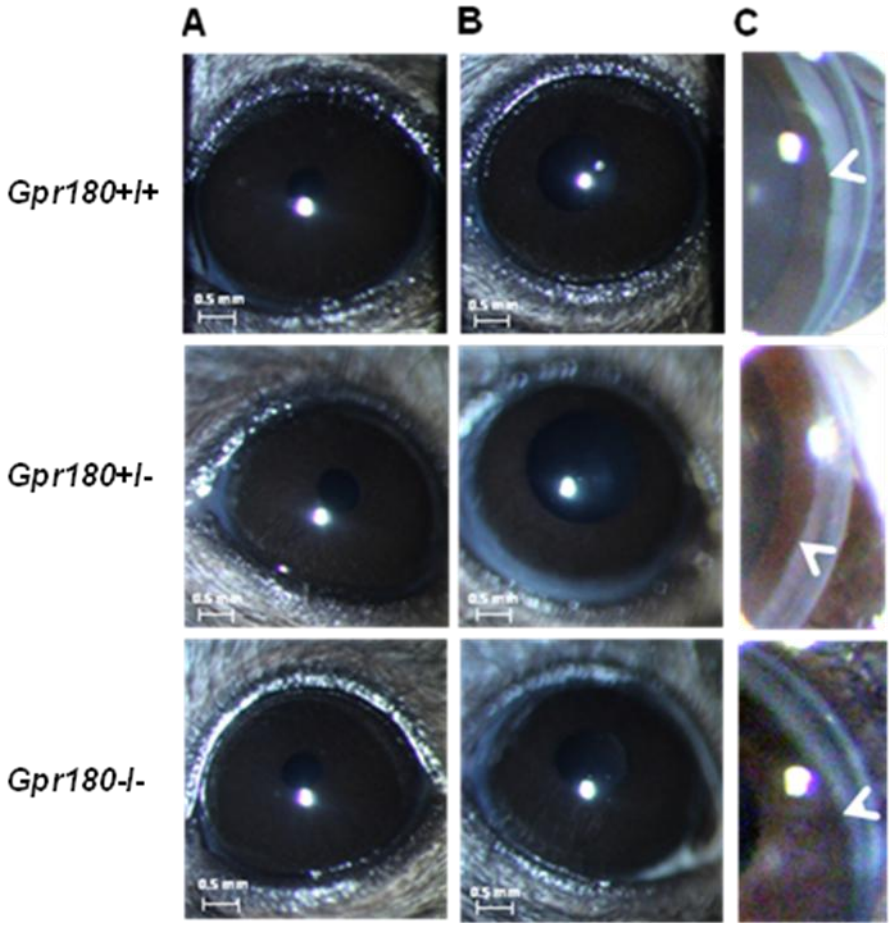

Figure S8. Iris phenotype of the *Gpr180*-null mice compared to heterozygote and wildtype animals. (A) The pupil diameter was invariably of 0.5 mm in the *Gpr180 -/-*, *Gpr180 +/-* and wildtype mice (n = 5 for each group). **(B)** Mydriasis upon 10 min treatment with neosinephrin 10% was highly variable in all animal groups (pupillary diameter ranging from 0.75 to 1.1 mm). **(C)** Gonioscopy reveals no difference in the iridocorneal line (arrow heads) between *Gpr180 -/-*, *Gpr180 +/-* and wildtype mice.

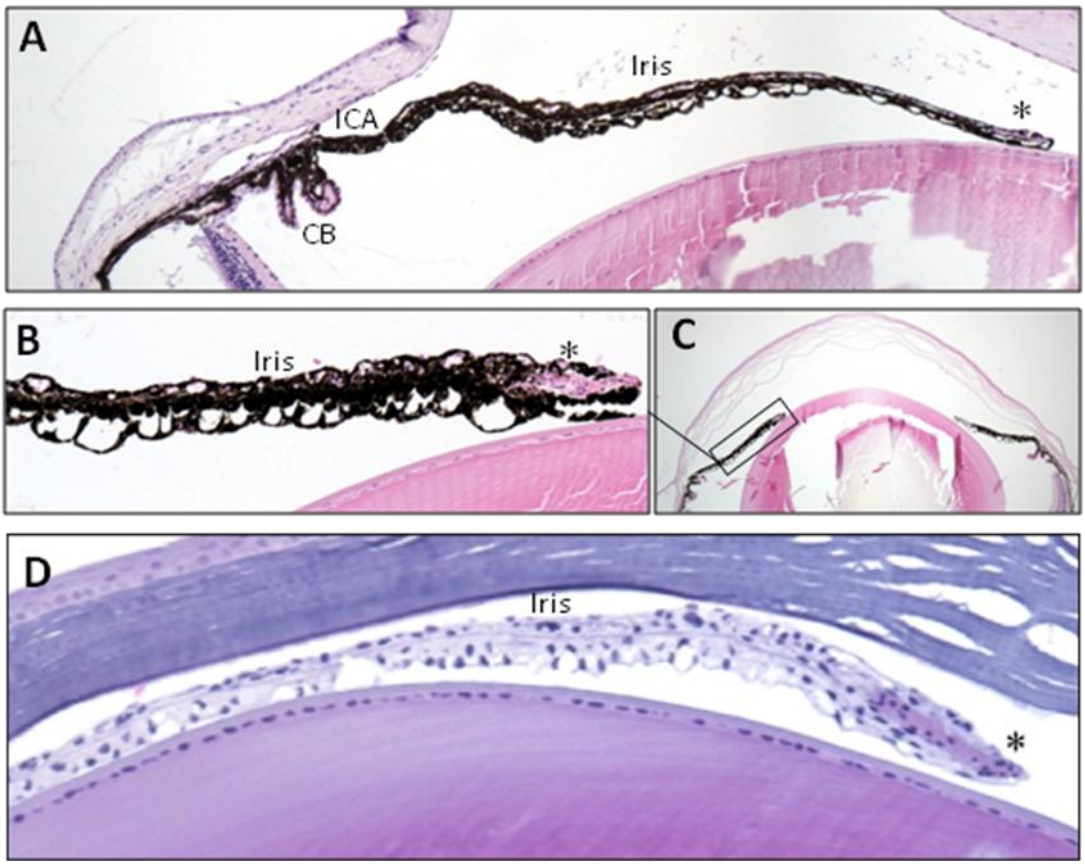

Figure S9. Routine histopathological evaluation of *Gpr180*-null mice iris. After enucleation, eye globes were immediately fixed in 10% buffered formalin before being automatically processed and embedded in paraffin. Four-micrometer paraffin-embedded sections were dewaxed in toluene and rehydrated through acetone bath to deionized water. Routine light microscopy evaluation was performed after haematoxylin and eosin staining **(A-C)** or Masson trichroma staining of sections bleached for melanin of uveal pigments, using hydrogen peroxide (H2O2) in phosphate saline buffer 0.05M, pH 7.4, at 55°C for 50 minutes **(D)**. Anterior uveal structures (iris, ciliary body (CB) and iridocorneal angle (ICA) of *Gpr180*-null mice were morphologically similar to wildtype and heterozygote animals. Iris constrictor muscle (∗) was prominent while iris dilator was not possible to identify in any of the animals.

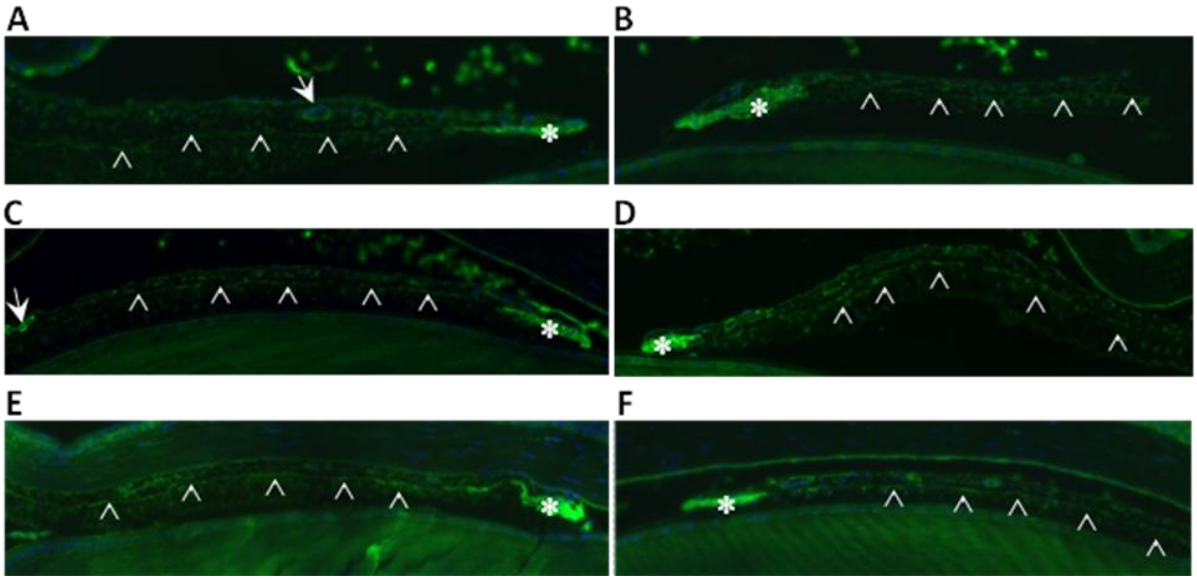

Figure S10. Alpha-smooth muscle actin (αSMA) immunostaining of wildtype, *gpr180*+/- and *grp180*-null mice. Four-micrometer dewaxed sections of wildtype **(A-B)**, *Gpr180*+/- **(C-D)** and *Grp180*-/- **(E-F)** mice were incubated with mouse monoclonal anti-monoclonal αSMA antibody (1:25, M0635, Dako) for 25 min at room temperature and using ARK kit (Dako K3954) according to manufacturer's recommendations. After washes, sections were then incubated with Alexa 488 conjugated goat anti-mouse IgG (1:100 in PBT (PBS + 0.15% BSA + 0.1% Tween 20), Molecular Probes, Eugene, OR, USA) for 30 minutes at 37°C in a humid chamber. Fluorescent anti-alpha SMA immunohistochemistry allowed to clearly identify iris constrictor muscle (∗), outlined vascular arterial structures in iris stroma (➔), and few thin muscular fibers in ciliary body. The iris dilator appears as a discontinuous discrete staining at the base of the posterior bilayered iris epithelium (arrow head), in wildtype, *Grp180*+/- and *Gpr180*-null mice.

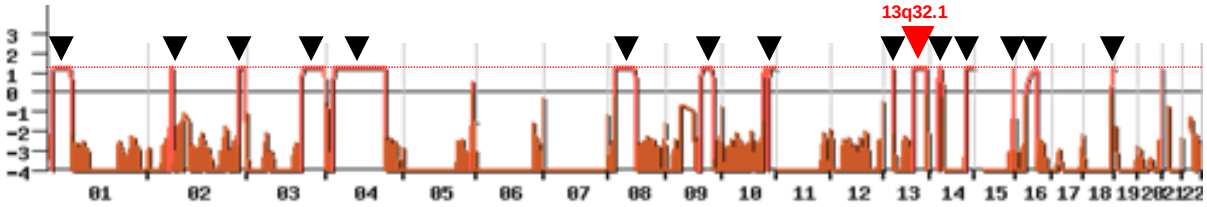

Figure S11. Full parametric linkage analysis of family FR3 using a combination of Affymetrix GeneChip Human Mapping 10K 2.0 Arrays. Parametric LOD scores were calculated with the MERLIN software program. Arrows point regions where the LOD scores reach the maximum value which can obtained in the family (red line). The red arrow points the MCOR region on chromosome 13q32.1.

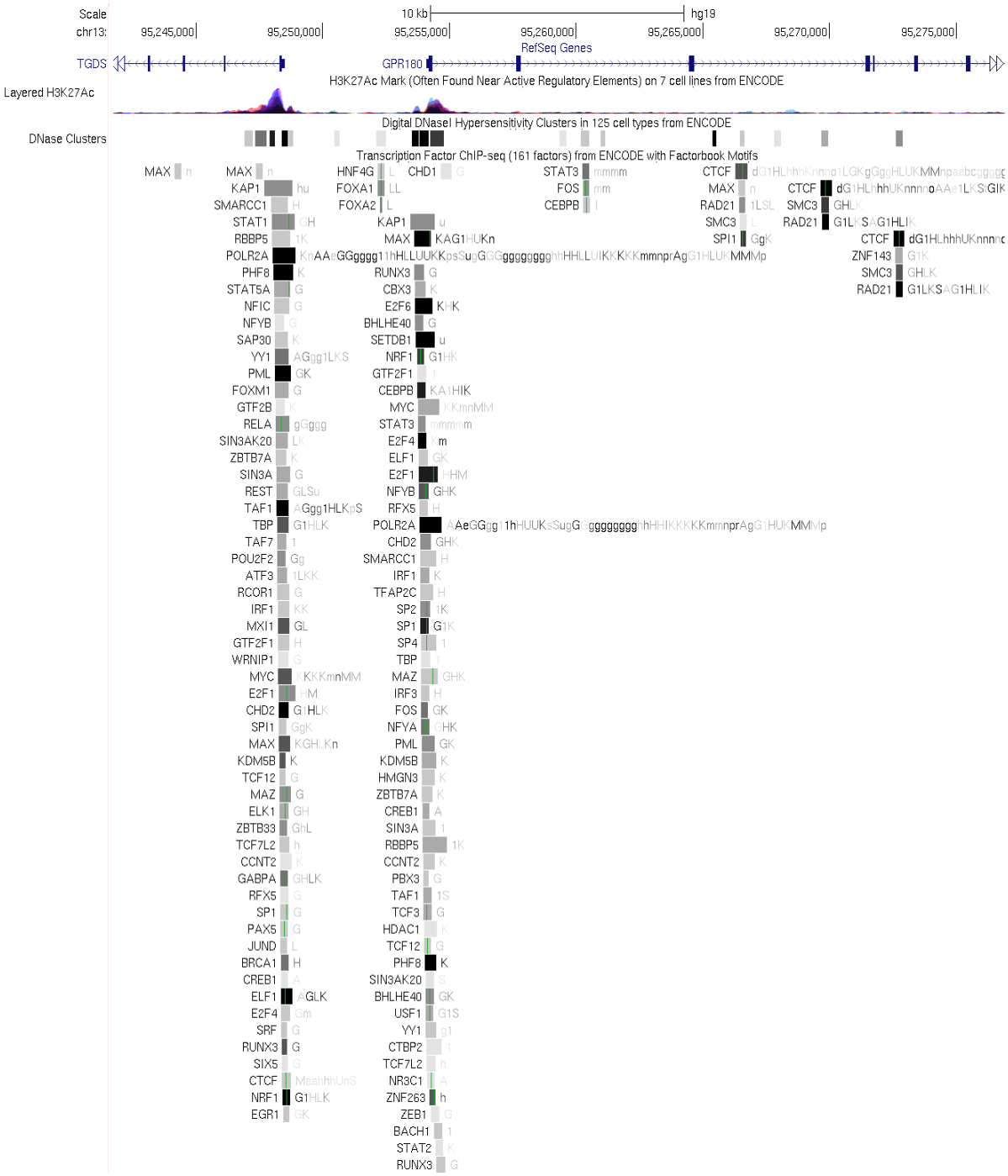

Figure S12. Overview of transcription factor binding sites lying within the minimal 13q32.1 MCOR deletion (chr13:95,241,606-95,276,905; hg19). The RefSeq Genes Track is displayed at the top and the Transcription factors CHIP-seq from ENCODE is shown at the bottom.

	JP1_III6	JP1_III7	JP1_III6 X JP1_III7
Coverage	185X	184X	-
Total variants (>5 of depth and >0.2 of fraction)	142,152	145,070	92,834
Variants with frequency < 1% or unknown in dbSNP135	13,196	15,122	5,428
Heterozygote variants	9,644	10,826	3,603
Acceptor/donor splice site, nonsense, indel, missense variants	484	556	228
Acceptor/donor splice site, nonsense, indel, possibly/probably damaging[a]	229	260	80
Variants mapping inside a candidate region (Figure 1S)	3	5	3[b]

a. Predictions according to Polyphen2

b. *TUSC1*_chr9:25678195-25678195 +CGC (exon1:c.124_125insGCG, p.S42delinsSG; NM_001004125); *HRCT1*_chr9:35906598-35906600 -ACC (exon1:c.314_316delACC: p.105_106del; NM_001039792.1); and *UNC13B*_chr9:35403470-35403470 C>T (p.A1455V; NM_006377.3)

Table S1. Whole exome sequencing results in family JP1. JP1_III6 and JP1_III7 exomes were captured from genomic DNA (1 μg) with in-solution enrichment methodology using the company's biotinylated oligonucleotide probe library (SureSelect Human All Exon 50 Mb Kits Version 3, Agilent, Santa Clara, CA, USA). Each genomic DNA was then sequenced on a sequencer as paired-end 100 bases (Illumina HISEQ2000, Illumina, San Diego, USA). Sequences were aligned to the human genome reference sequence (hg19 assembly). The coverage was calculated as total reads/total genomic lengths. SNPs were called on the basis of the allele calls and read depth using the SAMtools (http://samtools.sourceforge.net/). Genetic variation annotation was performed by the ANNOVAR (http://www.openbioinformatics.org/annovar/). Considering that MCOR is rare dominant disease, we assumed that affected individuals were likely heterozygote for variants absent or <1% minor allele frequency in the dbSNP135. Consensus splice site changes, insertion/deletion and nonsynonymous variants (nonsenses, and probably/possibly damaging missense variants as predicted by Polyphen2) shared by the two affected individuals were selected. Inspection for variants in the candidate regions pointed by linkage analysis (Figure S1), detected one indel, one in-frame deletion and one missense change in the chr9:1-85756778 interval: *TUSC1* [MIM610529], *HRCT1* (NM_001039792.1) and *UNC13B* [MIM605836], code for a tumor suppressor candidate, histidine rich carboxyl terminus 1, and a protein important for synaptic vesicle exocytosis, respectively. Corresponding amino acids, p.S42 in *TUSC1* and p.H105 in *HRCT1* are located in single amino acid repetitive sequences, suggesting length polymorphisms. Variants in these genes are unlikely to cause MCOR.

Family	Centromeric primer (5'-3')	Telomeric primer (5'-3')	Size (bp)
FR1	tcccaaagattgaggcattc	aaacttcaaatttatctgcttattgg	1098
FR2	cagcaagtgttggcaagcat	aaacttcaaatttatctgcttattgg	2297
JP1	tgctagctaagtcttgccca	aagtgaagggatcgtgcaga	1271
JP2	tgtgtccctctagagaaccctaa	gccctcacgtagcttttgat	1797
MX1, MX2	ggagaatcatgcctttggaa	ggcactgatgttgaatgcgt	1304

Table S2. Sequences of primer pairs used to amplify the intervening segments in MCOR affected individuals harboring 13q32.1 interstitial deletions. The sizes of intervening segments are given.

Gene	Exon	Forward primers (5'-3')	Reverse primers (5'-3')	Size (pb)
TGDS	2	6FAM_tgattgtctctttagtggaaga	gagcctctgaattgctaaaatga	184
GPR180	2	6FAM_caggaatggctaaagctacagc	tgggattatgctgtcaggaa	184
CFTR	25	6FAM_gcttgagtgtttttaactctgtgg	gggttcatcaagcagcaaga	204

Table S3. Primer sequences and sizes of *TGDS*, *GPR180* and *CFTR* amplicons used for QMPSF analysis. The forward primers have been labeled using the 6FAM fluorophore to allow analysis on an automated ABI3130 sequencer.

				Proximal breakpoint region			Distal breakpoint region				
Patient code	**Chromosomal position (hg19)**	**Size (kb)**	**Micro-homology (bp)**	**Repetitive element**	**Number of sequence motifs**	**Number of non-B DNA conformation prediction motifs[a]**	**Repetitive element**	**Number of sequence motifs**	**Number of non-B DNA conformation prediction motifs[a]**	**Sequence identity between repetitive elements**	**Potential molecular mechanism**
FR1	chr13:95,227,374-95,277,864	50.5	2	-	8	-	L1MC4a	3	1	-	FoSTeS/MMBIR/NHEJ
FR2	chr13:95,241,661-95,276,905	35.2	37	AluY	9	-	AluY	9	-	83%	NAHR/FoSTeS/MMBIR/ MMEJ
JP1	chr13:95,228,262-95,300,908	72.6	1	MER104	10	-	MLT1E1A	3	-	-	FoSTeS/MMBIR/NHEJ
JP2	chr13:95,236,251-95,309,380	73.1	-	L1MC5	5	-	Tigger4	7	-	-	FoSTeS/MMBIR/NHEJ
MX1 & MX2	chr13:95,225,217-95,305,083	79.9	2	ERV3-16A3_I-int	7	-	L1MC5	12	-	-	FoSTeS/MMBIR/NHEJ

a. Non-B DNA conformations should be located at both sides of the junction or overlapping the junction

Table S4. Overview of bioinformatic analysis results for the MCOR deletion breakpoints and surrounding genomic architecture.

Chromosome:position_variant	Protein consequence	Allele Count	Allele Number	Number of Homozygotes	Allele Frequency
13:95254225_G/A	p.Trp15Ter	1	11290	0	0.00008857
13:95254299_C/T	p.Gln40Ter	1	17616	0	0.00005677
13:95271542_T/A	p.Leu215Ter	2	122854	0	0.00001628
13:95271735_G/T	p.Gly234Ter	1	122540	0	0.000008161
13:95278239_T/A	p.Leu369Ter	1	122674	0	0.000008152
13:95278286_C/T	p.Gln385Ter	3	122444	0	0.00002450
13:95271434_T/TA	p.Val180SerfsTer18	1	122770	0	0.000008145
13:95273380_T/TATGC	p.Gly265HisfsTer45	1	122930	0	0.000008135
13:95273411_GA/G	p.Lys273SerfsTer24	5	122932	1	0.00004067
13:95275395_T/TA	p.Ile310AsnfsTer5	3	122712	0	0.00002445
13:95275491_C/CT	p.Tyr342LeufsTer41	1	122908	0	0.000008136
13:95279324_CTCTT/C	p.Phe409CysfsTer15	1	122876	0	0.000008138

Table S5: Rare *GPR180* variants predicted to truncate the protein. Inspection of ExAC, EVS, 1000Genome and dbSNP datasets pointed 12 nonsense and frameshift variants in the ExAC database, including one homozygote change, which reality needs to be demonstrated by Sanger sequencing.

Exon	Forward primer (5'-3')	Reverse primer (5'-3')
1	ggcctctgactggtgaatgt	aggtgaggctggggaagt
2	ttgcttctgaatgttgtgttca	tgggattatgctgtcaggaa
3	cacaaggtcttggatttctgag	ggaaacacaggttgctttca
4	ccccaaggtacaaaattgtttaag	gcaagcataattttggtggact
5	tcaaaaccactaaaactgtgttca	tcctgttctcagtcaagctgat
6	tttgaaaatggctttttgtgg	tgacacaaattgtagaagctcaga
7	aaaattcattttgtctagcttaggg	tcccaaagaaaccagaacca
8	ggcctgttgaggttaatcaga	aaacttcaaatttatctgcttattgg
9	tccttaaacaattagagttctgagca	atgctctgctttcgctgttc

Table S6. Primer pairs used to screen the *GPR180* gene for mutations in individuals with goniodysgenesis.